

H. Bounechba, A. Boussaid, A. Bouzid

### Experimental validation of fuzzy logic controller based on voltage perturbation algorithm in battery storage photovoltaic system

**Introduction.** Solar photovoltaic (PV) has recently become very important especially in electrical power applications for countries with high luminosity because it is an effectively unlimited available energy resource. Depending on solar radiation and temperature, the PV generator has a non-linear characteristic with a maximum power point (MPP). **The novelty** is the efficiency improvement of a PV energy module, it is necessary to track the MPP of the PV array regardless of temperature or irradiation circumstances. **Purpose.** This paper presents the modeling and the digitally simulation under MATLAB/Simulink of a Fuzzy Logic Controller based on Voltage Perturbation Algorithm (FLC-VPA) applied to PV battery charging system, which consists of PV module, DC-DC boost converter, MPP tracking (MPPT) unit and battery storage. **Methods.** The DSP1104 is then used to experimentally implement this MPPT algorithm for real-time driving. **The obtained results** show the high precision of the proposed FLC-VPA MPPT around the optimal point compared to the conventional VPA under stable and changing meteorological conditions. **Practical value.** The experimental results approve the effectiveness and validity of the proposed total control system in the PV system. References 30, tables 3, figures 17.

**Key words:** maximum power point, fuzzy logic controller based on voltage perturbation algorithm, battery, boost converter.

**Вступ.** Сонячна фотоелектрична (PV) енергія останнім часом стала дуже важливою, особливо в електроенергетиці в країнах з високим сонячним освітленням, оскільки вона є фактично необмеженим доступним енергетичним ресурсом. Залежно від сонячного випромінювання та температури, PV генератор має нелінійну характеристику з точкою максимальної потужності (MPP). **Новизною** є підвищення ефективності PV енергетичного модуля, що необхідно відстежувати MPP PV батареї незалежно від температури або умов опромінення. **Мета.** У цій статті представлено моделювання та цифрове моделювання в рамках MATLAB/Simulink контролера нечіткої логіки на основі алгоритму збурення напруги (FLC-VPA), що застосовується до системи зарядки PV батарей, яка складається з PV модуля, DC-DC підвищувального перетворювача, системи MPP (MPPT) та акумуляторної батареї. **Методи.** DSP1104 використовується для експериментальної реалізації цього MPPT алгоритму для режиму реального часу. **Отримані результати** показують високу точність пропонованого FLC-VPA MPPT біля оптимальної точки порівняно з традиційним VPA у стабільних та мінливих метеорологічних умовах. **Практична цінність.** Результати експериментів підтверджують ефективність та обґрунтованість запропонованої системи контролю у PV системі. Бібл. 30, табл. 3, рис. 17.

**Ключові слова:** точка максимальної потужності, контролер нечіткої логіки на основі алгоритму збурення напруги, акумулятор, підвищувальний перетворювач.

Abbreviations

ANN	Artificial Neural Network	MPPT	Maximum Power Point Tracking
FOCV	Fractional Open-Circuit Voltage	P&O	Perturb and Observe
FSCC	Fractional Short-Circuit Current	PV	Photovoltaic
FLC-VPA	Fuzzy Logic Controller based on Voltage Perturbation Algorithm	PWM	Pulse Width Modulated
FLC	Fuzzy Logic Controller	STC	Standard Test Conditions
INC	Incremental Conductivity	VPA	Voltage Perturbation Algorithm
MPP	Maximum Power Point		

**Introduction.** Renewable energies are an effective solution to eliminating greenhouse gas emissions. Among the promising resources of production (wind, hydro and so on), PV cells have become very important as they are one of the most suitable and successful renewable sources in the production of electricity due to its advantages such as no fuel cost, and no noise; and because the solar cell is a semiconductor device, it needs very little maintenance and so on.

The PV module directly converts solar energy into electricity. The output value of these PV modules varies according to environmental conditions such as radiation and the temperature (Fig 1). The solar modules have distinctive characteristics, including that the maximum value of the available energy is available only in one operating point that has a specific voltage and current, called the MPP, whose position changes as a function of radiation and temperature of the solar module so that the used load (Fig. 2).

The major drawback of PV systems is the relatively expensive cost of this kind of energy. To get rid of this problem, we must make the solar panels work at maximum power to increase the energy efficiency of these systems. This requires a tracking mechanism of this point so that the maximum power is generated continuously.

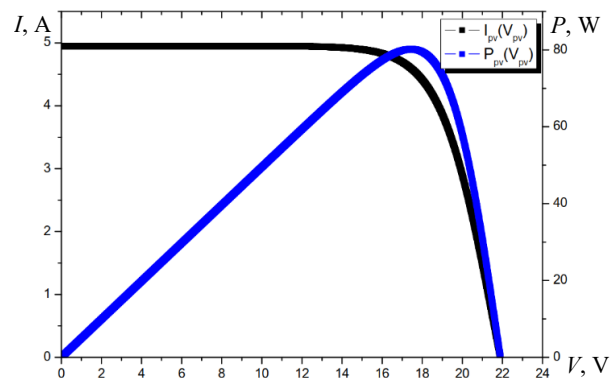


Fig. 1. Current and power curves under 1000 W/m<sup>2</sup> and 25 °C

MPPT enables us to control the operating point by regulating the duty cycle converter circuit connected between the PV generator and the load or battery storage.

Various MPPT methods have been developed and executed: P&O [1], INC [2], FOCV [3] and FSCC [4]. The existing methods have one or more defects, such as costly, difficult to achieve, plurality of sensors, high complexity, easy to instability. The first two are used in many PV systems more largely than others because of their simple implementation.

© H. Bounechba, A. Boussaid, A. Bouzid

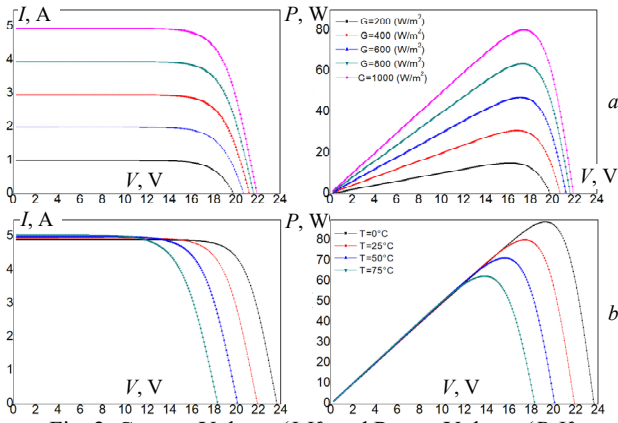


Fig. 2. Current-Voltage ( $I$ - $V$ ) and Power-Voltage ( $P$ - $V$ ) characteristics:  $a$  – temperature  $T = 25$  °C and different levels of irradiance  $G$ ;  $b$  – at irradiance  $G = 1000$  W/m<sup>2</sup> and different temperatures  $T$

When the control parameter is increased or decreased to a small extent (step size) in the P&O method, a disturbance occurs at the PV generator operating point. We measure the PV external energy before and after the disturbance, if there is an increase in the power, the algorithm continues to perturb order in the same way; if it is the other way around, the system will perturb in the opposite way [5], and this algorithm can be described based on the nature of the control variable you use [6]:

- 1) *voltage* – Voltage Perturbation Algorithm;
- 2) *current* – Current Perturbation Algorithm;
- 3) *duty cycle* – Duty Cycle Perturbation Algorithm.

To determine the unit operating point on both sides of the MPP we derive the power from the voltage and then approximate this point from the MPP by adjusting the duty cycle. This method is called the INC method.

In the presence of uniform radiation the previous two methods work effectively because there is only one MPP in this case however, boot P&O and INC become ineffective under rapid change in the atmosphere as well as power fluctuations at the MPP [7–9].

FOCV and FSCC methods are simple methods for obtaining maximum power, but they are inaccurate because they give only an approximation of the constant ratio between optimum voltage and open circuit voltage or between optimum current and short circuit current for the PV panel. This makes the efficiency of the PV system weak and energy loss, especially that the MPP varies with the level of radiation and temperature [10].

FLC and ANN are smart methods and techniques that have recently been used in the literature [11–14]. ANN presents some drawbacks despite its good performance, especially in the case of rapid fluctuations in weather conditions. Hence, its robustness requires a massive database [15]. The proposed FLC-VPA method is better than MPPT methods used in a several applications [16–20] because it is easy to design, robust and requires no exact model.

**The goal of the paper** expressed in proposing a fuzzy logic controller based on the principal of the well-known voltage perturbation algorithm. The last-mentioned algorithm uses a fixed step size, if it is taken to large, the power perturbation increases. The main contribution of this paper is the introduction of a FLC-

VPA that uses a variable step size to avoid the large time response of VPA when the step size chosen too small.

**PV module.** To carry out the simulation and the experimental part we chose the STP080S-80 12/Sb PV module. The module is made up of 36 monocrystalline silicon solar cells connected in series to produce a maximum power of 80 W. Solar cells are typically studied under STC, where the mean solar spectrum value is AM1.5, and at an estimated irradiance of 1000 W/m<sup>2</sup>, with the cell temperature set as 25 °C.

The prototypical involves a current generator to simulate the flow of incident light and a diode for the polarization of cells (Fig. 3).

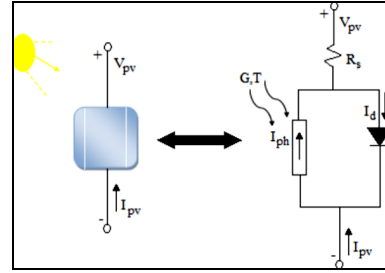


Fig. 3. Equivalent schematic of the PV cell

To account for physical phenomena at the cell level, the model is supplemented with a series resistor  $R_s$ . The behavior of a PV cell with a silicon based PN junction can be characterized by the equation in statics [21]:

$$I_{pv} = I_{ph} - I_d. \quad (1)$$

The diode current is given by:

$$I_d = I_s \cdot \left[ \exp \left( q \cdot \frac{V_{pv} + R_s I_{pv}}{A \cdot k \cdot T} \right) - 1 \right], \quad (2)$$

where:  $q$  is the electron charge ( $q = 1.602 \cdot 10^{-19}$  C);  $k$  is the Boltzmann constant ( $k = 1.38 \cdot 10^{-23}$  J/K);  $A$  is the diode ideality;  $I_s$  is the reverse diode saturation current;  $R_s$  is the series resistance of the cell;  $T$  is the temperature, K;  $V_{pv}$ ,  $I_{pv}$  are the output voltage and current of the solar cell, respectively.

The saturation current  $I_s$  varying with temperature, which is described as:

$$I_s = I_{so} \cdot \left( \frac{T}{T_{ref}} \right)^{\frac{3}{A}} \cdot \exp \left[ \left( -\frac{E_g}{A \cdot k} \right) \cdot \left( \frac{1}{T} - \frac{1}{T_{nom}} \right) \right]; \quad (3)$$

$$I_{so} = \frac{I_{sc\_nom}}{\exp \left( q \cdot \frac{V_{oc\_nom}}{A \cdot k \cdot T_{nom}} \right) - 1}, \quad (4)$$

where  $I_{ph}$  is the generated photo-current, which is primarily determined by irradiance  $G$  and cell temperature  $T$  as follows:

$$I_{ph} = I_{ph\_nom} \cdot [1 + \alpha(T - T_{nom})]; \quad (5)$$

$$I_{ph\_nom} = I_{sc\_nom} \cdot \frac{G}{G_{nom}}; \quad (6)$$

where  $G_{nom}$  is the nominal irradiance;  $T_{nom}$  is the nominal temperature;  $I_{sc\_nom}$  is the nominal short circuit current;  $V_{oc\_nom}$  is the nominal open circuit voltage of PV panel at STCs.

The Suntech A STP080S-12/Bb PV panel was utilized in the simulation, and the data for the PV module can be seen in Table 1.

Table 1  
Parameter condition of STP080S-12/Bb PV module

Parameter	Value
Maximum power $P_{max}$ , W	80
Maximum voltage $V_{max}$ , V	17.5
Current at the maximum power $I_{max}$ , A	4.58
Open circuit voltage $V_{oc}$ , V	21.9
Short circuit current $I_{sc}$ , A	4.95

The maximum voltage  $V_{max}$  and maximum current  $I_{max}$  to the MPP, the open circuit voltage  $V_{oc}$ , the short circuit current  $I_{sc}$ , and the slopes of the curves  $I-V$  near  $V_{oc}$  and  $I_{sc}$  are used to determine the ideal factor and series resistance for a specific solar radiation and temperature [22].

**DC/DC converter.** A chopper is a DC/DC converter that converts DC energy at one voltage (or current) level to DC energy at a different voltage (or current). Depending on the load voltage, numerous DC/DC converters can be connected to the PV generator (buck, boost and buck boost).

The employed structure of the DC-DC boost chopper in this research is shown in Fig. 4, where S is the switch, L is the boost inductor and C is the filter capacitor.

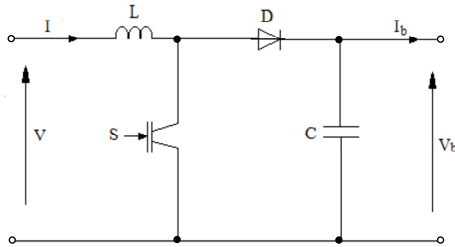


Fig. 4. Scheme of the boost converter

Equation (7) is the energy model of the used boost converter:

$$\frac{d}{dt} \begin{bmatrix} V_b \\ I \end{bmatrix} = \begin{bmatrix} 0 & (1-\alpha)/C \\ (\alpha-1)/L & 0 \end{bmatrix} \begin{bmatrix} V_b \\ I \end{bmatrix} + \begin{bmatrix} 0 & -1/C \\ 1/L & 0 \end{bmatrix} \begin{bmatrix} V \\ I_b \end{bmatrix}, \quad (7)$$

where  $I$ ,  $V$ ,  $V_b$ ,  $I_b$  and  $\alpha$  are the input current, input voltage, output voltage, output current and duty ratio of boost converter, respectively. Because the output voltage of a DC-DC boost converter is always higher than the input voltage, it can be used to connect low module voltages to high load/battery voltages [23].

By adjusting the switching duty cycle  $\alpha$ , an IGBT can boost the PV module's output voltage:

$$V_b = V / (1 - \alpha). \quad (8)$$

When the switch S is turned on, current travels from the input source through the inductor L to the IGBT, storing energy in the inductor as a result. The energy stored in the inductor is released through the diode to the C and the load when the switch S is turned off.

The boost converter specifications are shown in Table 2.

Boost converter parameters

Component	Specification	Value
IGBT	1 × IRGPC60K	600 V, 41 A, 15 V at 125 °C
Schottky diode	1 × GI BYW29-150 9616	150V, 8 A, 0.8 V at 150 °C
L	2 × LEYBOLD 56214 parallel	0.011 mH, 2.5 A
C	2 × REA series	47 μF, 400 V

Table 2

**Battery modeling.** Batteries are complicated electrochemical devices that use chemical bonds to store electrical charge. Lead acid battery is generally used storage component in PV system. There are several lead battery models proposed, in this paper we have opted for the Thevenin model used in [24] (Fig. 5).

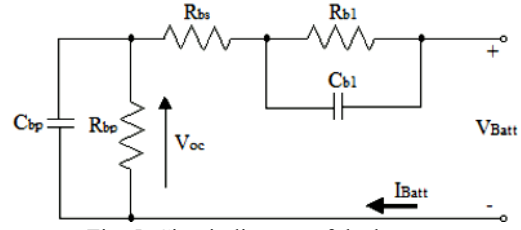


Fig. 5. Circuit diagram of the battery

The battery, on the other hand, is an energy storage element whose energy is measured in kWh. When a capacitor is used to mimic the battery unit, the following factors can be considered:

$$C_{bp} = \frac{2 \cdot E_b}{V_{max}^2 - V_{min}^2}, \quad (8)$$

where  $C_{bp}$  is the battery charge capacity;  $E_b$  is the energy given by the manufacturer of the battery, kWh;  $V_{max}$ ,  $V_{min}$  are the maximum and the minimum voltage of the battery in open circuit respectively.

The circuit in Fig. 5 describes the characteristics of a lead acid battery with a complete manner yet very simplified, this circuit expresses the input equivalent impedance  $Z_b$  by:

$$Z_b(s) = R_{bs} + \frac{R_{b1}}{R_{b1}C_{b1}s + 1} + \frac{R_{bp}}{R_{bp}C_{bp}s + 1}, \quad (9)$$

where  $R_{b1}$  and  $C_{b1}$  are the energy and voltage during charging and discharging using the parallel circuit; the resistance of  $R_{bp}$  is significant because the self-discharging current of a battery is minimal.

**VPA MPPT.** VPA is one of the easier online procedures can be realized by applying a disruption to the reference voltage. According to the flowchart (Fig. 6) VPA operates by periodically perturbing (increases or decreases) the module terminal voltage and estimates the power difference between the present and the past extracted power from the PV source such as  $V_{pv}(n)$ ,  $I_{pv}(n)$  and  $P_{pv}(n)$  are voltage, current and power of PV panel at  $n^{th}$  iteration, respectively.

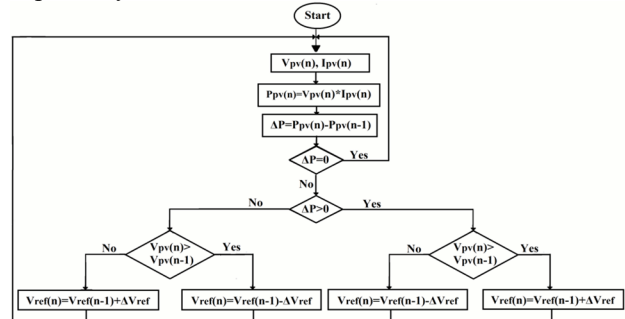


Fig. 6. Flow chart of the VPA MPPT

If the power difference is positive, the tracking is in the right direction and the perturbation direction will keep on (increase or decrease) in the next cycle.

However, the opposite perturbation direction will occur at a negative power difference; similarly, the next cycle is repeated until the MPP is tracked.

The choice of the perturbation step value ( $\Delta V_{ref}$ ) applied to the system, is very important because it is the responsible of oscillations and moreover the convergence speed to the final response. If a large perturbation step is used the algorithm will find the maximum value faster, nevertheless the quantity of power loss caused by the perturbation is high.

A modest perturbation step, on the other hand, can lessen the power loss caused by the perturbation while slowing down the system's tracking speed. This phenomenon is a term used to describe the trade-off between tracking speed and tracking precision [25].

**FLC-VPA MPPT controller.** Fuzzy systems are based on Lotfi Zadeh's fuzzy set theory and related techniques, which he pioneered in 1965. Because of their simplicity and effectiveness for both linear and nonlinear systems, they have been successfully applied in a variety of domains including control systems engineering, industrial automation, and optimization. FLCs which don't require the knowledge of an exact plant model, have recently been introduced in the following of the MPP in PV systems [26].

FLC-VPA method suggested in this research takes advantage of the VPA's simplicity as well as its ability to reduce the FLC's steady state oscillations. FLC-VPA technique examines the properties of PV panels before perturbing the operating voltage by an appropriate increment ( $\Delta V_{ref}$ ) to adjust the PV power. The power variation ( $\Delta P_{pv}$ ) might be in either a positive or negative direction.

The value of ( $\Delta P_{pv}$ ) can be huge or tiny. From here, the voltage variation ( $\Delta V_{ref}$ ) is increased or lowered in a small or large way in the direction that allows the power  $P_{pv}$  to be increased until the optimum is reached.

FLC-VPA MPPT controller, like conventional FLC, consists of 3 phases – fuzzification, rule processing unit and defuzzification (Fig. 7). The triangular and trapezoidal shapes were chosen for the fuzzy control because they consume less hardware memory and have a simpler parametric representation. The triangular version of this procedure's membership function assumes that there is only one main fuzzy subset for each input [27].

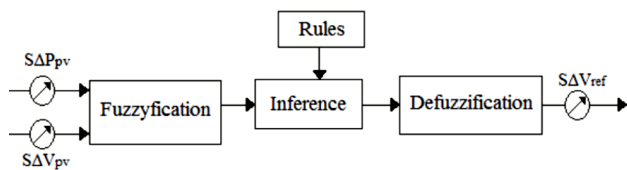


Fig. 7. Fuzzy controller structure

1. *Fuzzification.* The fuzzy control requires that variable used in describing the control rules has to be expressed in terms of fuzzy set notations with linguistic labels [28]. In this paper, the FLC-VPA MPPT method has two input variables, namely  $\Delta P_{pv}(n)$ ,  $\Delta V_{pv}(n)$ , and one output variable  $\Delta V_{ref}(n)$ ; at a sampling instant  $n$ , where the variable  $\Delta P_{pv}(n)$  and  $\Delta V_{pv}(n)$  are expressed as follows:

$$\Delta P_{pv} = P_{pv}(n) - P_{pv}(n-1); \quad (10)$$

$$\Delta V_{pv} = V_{pv}(n) - V_{pv}(n-1); \quad (11)$$

where  $P_{pv}(n)$  and  $V_{pv}(n)$  are the power and the voltage of the PV module.

The fuzzy sets for both inputs and output are: P (positive), N (negative), Z (zero), as shown in Fig. 8.

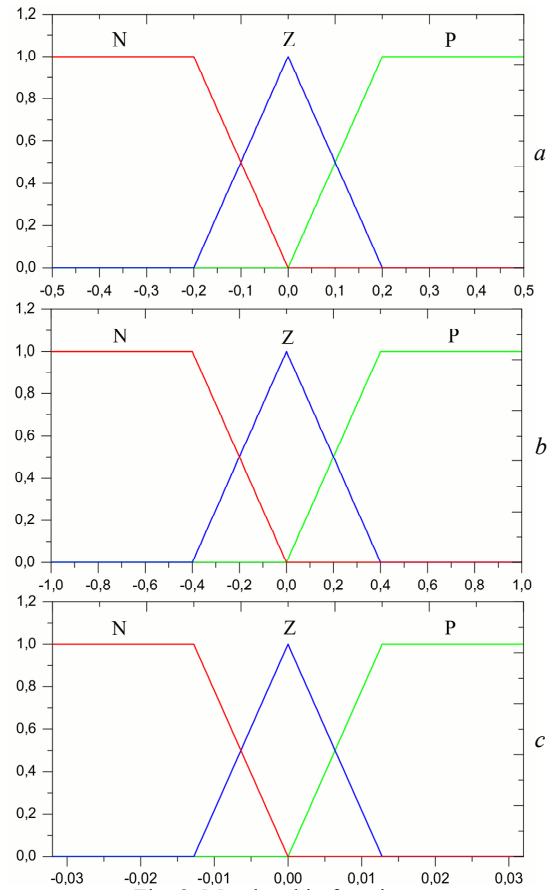


Fig. 8. Membership functions: a – input  $\Delta V_{pv}$ ; b – input  $\Delta P_{pv}$ ; c – output  $\Delta V_{ref}$

2. *Inference method.* The inference method used to determine the output of fuzzy logic controller. Several inference methods are discussed in literature include Compositional Rule of Inference, Generalized Modus Ponens and Sugeno inference method [29].

In this study Mamdani's inference method is employed because it was the most common method used in engineering application [30].

The composition operation is the method by which a control output is generated, the commonly applied method is MAX/MIN used in this article.

The membership function of every rule is given by the MIN operator and MAX operator. The construction of control rules to relate the fuzzy input to the fuzzy output depends on the knowledge base of the system dynamics. The control rules proposed is presented in Table 3. For one example, control rule in Table 3 is expressed as follows. «IF  $\Delta P_{pv}$  is P and  $\Delta V_{pv}$  is P THEN  $\Delta V_{ref}$  is P». This implies that «IF the power change is positive, AND the voltage variation is positive THEN the perturbation step will increase in the next cycle».

Table 3

		Control rules		
		$\Delta V_{pv}$	N	Z
$\Delta P_{pv}$	N	P	Z	N
	Z	N	Z	P
	P	N	Z	P

3. *Defuzzification.* After evaluating the rules, the FLC-VPA's final step is to compute the output, which is

the perturbation step ( $\Delta V_{ref}$ ) with the defuzzification process.

The centroid approach, commonly known as the Center of Gravity method, is employed in this paper, because it has good averaging capabilities and gives decent results. The crisp value of the control output  $\Delta V_{ref}$  is calculated as:

$$\Delta V_{ref} = \frac{\sum_{j=1}^n W_j \Delta V_j}{\sum_{j=1}^n W_j}, \quad (12)$$

where  $n$  is the maximum number of effective rules;  $W_j$  is the weighting factor;  $V_j$  is the value corresponding to  $\Delta V_{ref}$  membership function.

This adjustment is added to the previous control voltage value to get the final control voltage:

$$V_{pv}(n) = V_{pv}(n-1) + \Delta V_{ref}(n). \quad (13)$$

The terminal and reference voltages were measured at each sample period, and the error  $e = (V_{ref} - V_{pv})$  was determined. FLC-VPA adjusts the reference voltage ( $V_{ref}$ ) for MPPT as previously stated. This voltage is the positive input (reference) to the PI controller, which conducts steady-state voltage control.

To get the terminal voltage to the desired value, a PWM generator is utilized to adjust the duty ratio of the converter. FLC-VPA controller is implemented in real-time for MPPT following the methods outlined above.

**Simulation results.** A simulation of a solar panel with 36 cells connected to a storage battery via a DC-DC boost converter with MPPT algorithms is used in this section. The DC input voltage is converted to the battery voltage level using a DC-DC boost converter. This research compares and contrasts the VPA and FLC-VPA MPPT algorithms for tracking of maximum power. We have combined the two improved methods shown above in Fig. 9 to evaluate their efficiency.

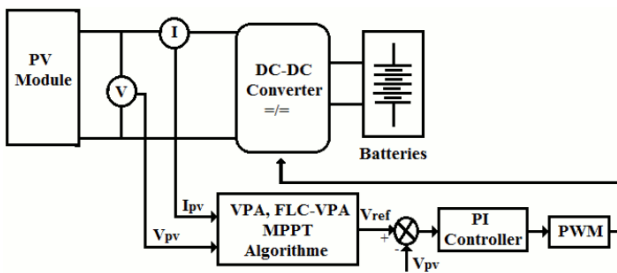


Fig. 9. Block diagram of the PV battery charging system

a) *PI controller effectiveness.* To improve the efficiency of the PI controller, the two MPPT algorithms studied in this paper was simulated under constant irradiance  $1000 \text{ W/m}^2$  and temperature  $25^\circ\text{C}$ .

Figure 10 shows that for VPA or FLC-VPA MPPT algorithms the PI loop provides overall system stability.

The error  $e$  in VPA is very large compared with the error of FLC-VPA because of the voltage reference perturbation.

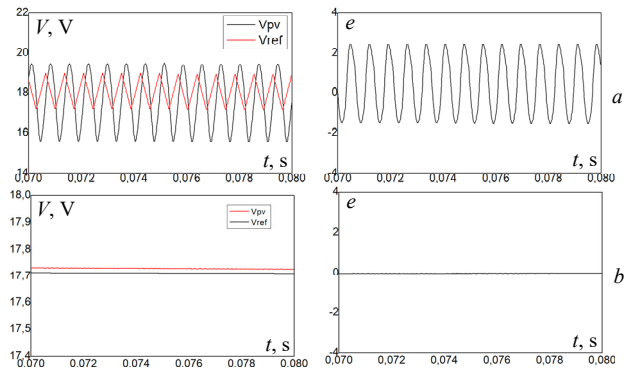


Fig. 10. PI controller efficiency for both controllers: a – VPA; b – FLC-VPA

b) *Irradiation influence.* Figure 11 depicts the simulation results by changing the solar irradiance disturbance from  $1000 \text{ W/m}^2$  to  $600 \text{ W/m}^2$  at a constant temperature of  $25^\circ\text{C}$ . When the simulation is started, both MPPT algorithms detect the maximum power available; although the detection of the maximum power is taking place, VPA and FLC-VPA generate the necessary control signals for the operation power of PV module follows the MPP with a minimum error.

The irradiation intensity abruptly rises to  $600 \text{ W/m}^2$  at  $t = 0.2 \text{ s}$ , causing a negative change, and the MPP search process is initialized to look for a new MPP. After determining the new MPP, the two MPPT algorithms investigated in this study operate the PV module at the new MPP.

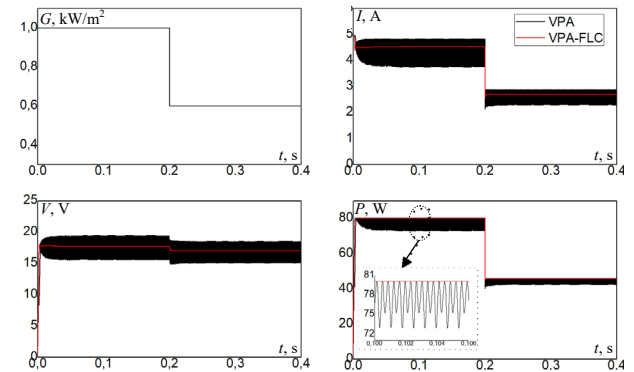


Fig. 11. Variations in irradiance have an impact on the management of both MPPT at a constant temperature of  $25^\circ\text{C}$

c) *Temperature influence.* We report in Fig. 12 the response of the two algorithms to a random variation of the temperature.

We note that for a quick variation of temperature, between a minimal value of  $15^\circ\text{C}$  and a maximum value of  $25^\circ\text{C}$ ; it's clear that the algorithm which adapts better is FLC-VPA. Thus, with this simulation tool, we have highlighted the fact that for fast step changes in temperature, the advantages of the FLC-VPA to the VPA by achievement of the MPP which is carried out instantaneously in the good direction without additional oscillations when the MPP is reached. And what enhance our study is that the power and the voltage of the PV module follow the variation of temperature conversely what is completely the opposite in the current PV module witch stay constant under temperature variation.

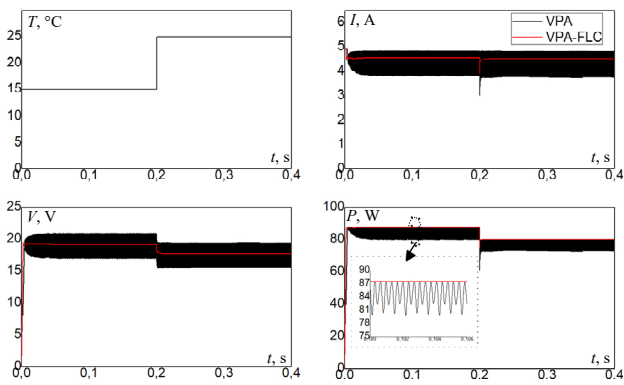


Fig. 12. The effect of temperature fluctuations on the control of both MPPT at a fixed irradiance of  $1000 \text{ W/m}^2$

**Experimental results.** A prototype PV battery charging system was created and tested for experimental verification. In this study, a STP080S-12/Bb PV module with a  $30^\circ$  and a maximum power of 80 W in standard irradiance and temperature was used. To draw the  $I_{pv}(V_{pv})$  and  $P_{pv}(V_{pv})$  characteristics of STP080S-12/Bb module the circuit shown in Fig. 13 is used.

Two batteries in series each one is determined by nominal voltage of a battery ( $12 V_{dc}$ ) and battery capacity (100 Ah) compose the energy storage component.

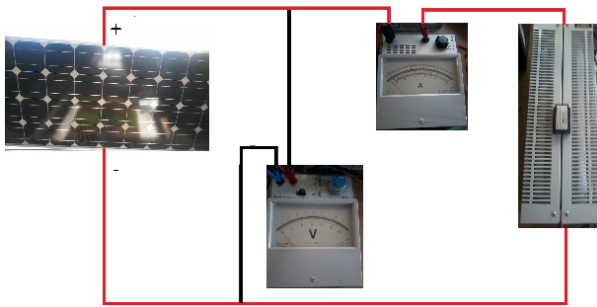


Fig. 13. Circuit measurement of  $I_{pv}(V_{pv})$  and  $P_{pv}(V_{pv})$  of STP080S-12/Bb module

The PV power system consists also of a DC-DC boost converter, which has the parameters summarized in Table 2 to step up the PV module voltage. Figure 14 depicts the synoptic diagram of this PV system.

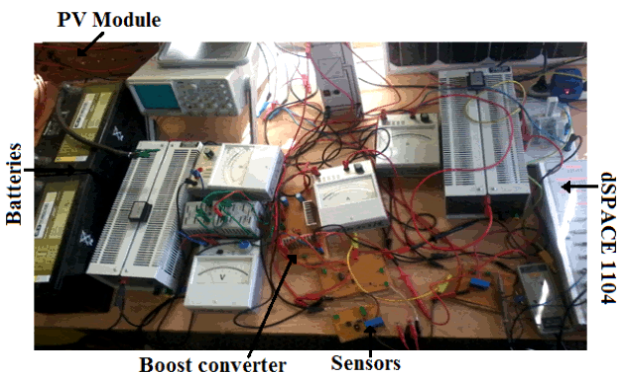


Fig. 14. Experimental setup of the PV battery charging system

The control platform for assessing MPPT algorithms was a dSPACE 1104 controller board. Allowing MATLAB/Simulink to communicate with real-world hardware. This is accomplished by utilizing dSPACE

interface blocks' input/output (I/O); the inputs are analog to digital converter (ADC) and the outputs are digital to analog converter (DAC). The voltage and current of the PV module are used as inputs to the dSPACE 1104 interface for the MPPT algorithms proposed in this work, and LEM sensors (LV25-P) and (LA25-P) are employed for data processing.

On MATLAB/Simulink model the MPPT method generate the reference voltage and is compared with the sensed PV module voltage which gives the modulating wave for the PWM after real-time simulation.

The output of the dSPACE 1104 is limited by 10 V, so we utilized an amplifier circuit to boost the output voltage to a level that could feed the IGBT (15 V). When the pulses are augmented, they pass via an isolated circuit that separates the power and control circuits. For noise rejection from the module current and voltage feedback signals, low pass filters are used.

The PV array's nonlinear feature can be seen in the current and power curves (see Fig. 1). As a result, an MPPT algorithm must be implemented to force the system to function at MPP all the time.

In this paper two MPPT algorithms are carried out, therefore, to confirm the efficiency of the algorithms a real time simulation using DSP1104 is used.

Figure 15 shows the current, power and voltage of PV module under constant temperature and irradiance using VPA with 0.5 V of perturbation step. In the solar irradiation  $779 \text{ W/m}^2$ , PV output current is ranging from 1.5 A to 4 A and the rate of change of the PV module voltage is about 12 V results a PV power output perturbs between 30 W and 51 W, all this perturbation creates power loss in the PV system.

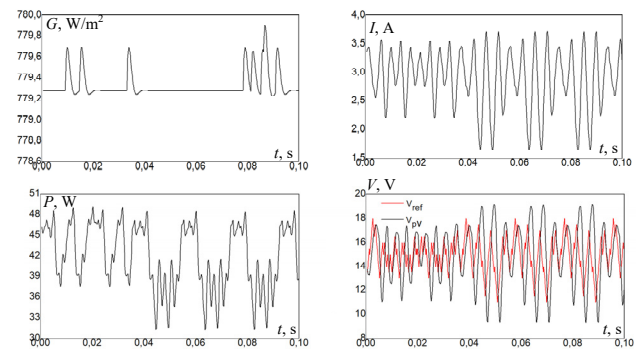


Fig. 15. Real time simulation results using VPA under constant irradiance and temperature

To reduce the perturbation, we can minimize the perturbation step value but that can provoke a divergence of the system after a few seconds of the beginning of the real time simulation.

The system is working with an average power of 51 W, which corresponds to the maximum power of the PV module under  $780 \text{ W/m}^2$ , and this power is practically constant (Fig. 16). As a result, the system's operation in this state demonstrates the FLC-VPA method's efficiency tracking.

**Comparison of MPPT algorithms.** The boost converter is turned on inactive mode at first. As a result, the PV module is directly connected to the two 24 V storage batteries. The operational voltage and current of the PV module are 17.5 V and 1.9 A, respectively.

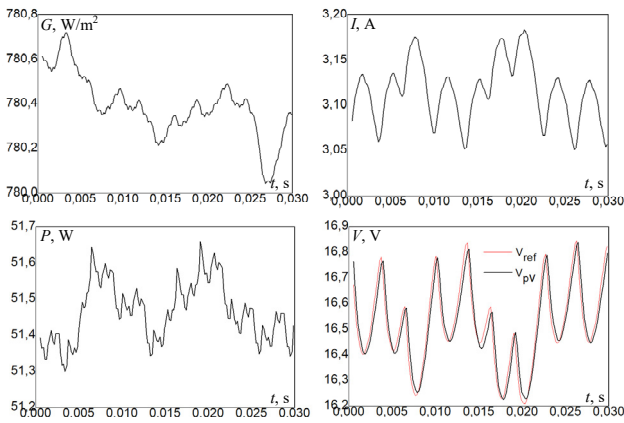


Fig. 16. Real time simulation results using FLC-VPA under constant irradiance and temperature

The irradiance measured is  $473 \text{ W/m}^2$ , both of algorithms optimize the PV system by make the PV module offer the maximum power, but the FLC-VPA is better than the VPA because this last present a very perturbed reference voltage and that's clear in the error curve.

When the FLC-VPA method is employed, the PV module power is  $33.5 \text{ W}$ , however when the VPA is applied, the power is balanced between  $25 \text{ W}$  and  $32.5 \text{ W}$ , resulting in significant power losses (Fig. 17). It should be emphasized that the VPA controls the system using oscillating signal responses, and hence may fail to achieve the optimization goal described in the introduction. The efficiency of the FLC-VPA system, as well as its ability to operate at maximum power, is demonstrated in this study.

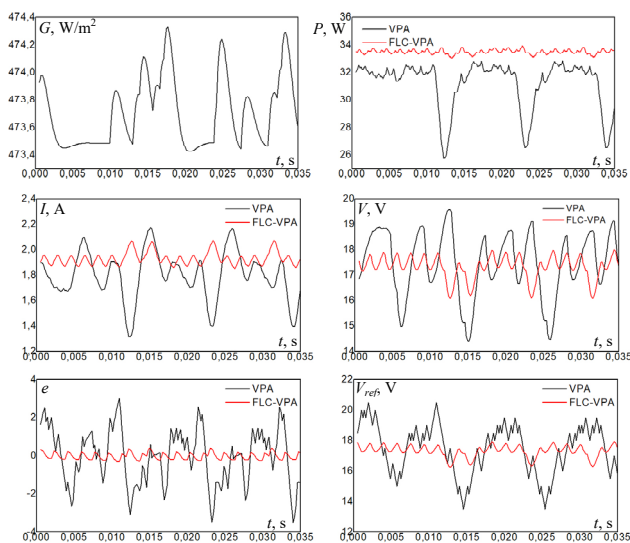


Fig. 17. Experimental results for both controllers showing system responses to a PV panel

**Conclusions.** In this research, we combine the traditional voltage perturbation algorithm with the fuzzy logic controller in the field of energy development with the goal of improvement the performance and maximizing the efficiency of solar modules by allowing them to operate at their maximum power. By incorporating the advantages of both algorithms, this controller increased the voltage perturbation algorithm's simplicity while also eliminating the complexity of the original fuzzy logic controller and ensuring the system's efficiency. The fuzzy logic based on voltage perturbation controller's

effectiveness for system optimization is demonstrated through simulation and experimental findings utilizing the control system card dSPACE1104.

**Conflict of interest.** The authors declare that they have no conflict of interest.

## REFERENCES

- Hafeez M.A., Naeem A., Akram M., Javed M.Y., Asghar A.B., Wang Y. A Novel Hybrid MPPT Technique Based on Harris Hawk Optimization (HHO) and Perturb and Observer (P&O) under Partial and Complex Partial Shading Conditions. *Energies*, 2022, vol. 15, no. 15, art. no. 5550. doi: <https://doi.org/10.3390/en15155550>
- Ibrahim M.H., Ang S.P., Dani M.N., Rahman M.I., Petra R., Sulthan S.M. Optimizing Step-Size of Perturb & Observe and Incremental Conductance MPPT Techniques Using PSO for Grid-Tied PV System. *IEEE Access*, 2023, vol. 11, pp. 13079-13090. doi: <https://doi.org/10.1109/ACCESS.2023.3242979>
- Hassan A., Bass O., Masoum M.A.S. An improved genetic algorithm based fractional open circuit voltage MPPT for solar PV systems. *Energy Reports*, 2023, vol. 9, pp. 1535-1548. doi: <https://doi.org/10.1016/j.egyr.2022.12.088>
- Claude Bertin Nzoundja Fapi, Wira P., Kamta M., Tchakounte H., Colicchio B. Simulation and dSPACE Hardware Implementation of an Improved Fractional Short-Circuit Current MPPT Algorithm for Photovoltaic System. *Applied Solar Energy*, 2021, vol. 57, no. 2, pp. 93-106. doi: <https://doi.org/10.3103/S0003701X21020080>
- Feroz Mirza A., Mansoor M., Ling Q., Khan M.I., Aldossary O.M. Advanced Variable Step Size Incremental Conductance MPPT for a Standalone PV System Utilizing a GA-Tuned PID Controller. *Energies*, 2020, vol. 13, no. 16, art. no. 4153. doi: <https://doi.org/10.3390/en13164153>
- Sibtain D., Gulzar M.M., Shahid K., Javed I., Murawwat S., Hussain M.M. Stability Analysis and Design of Variable Step-Size P&O Algorithm Based on Fuzzy Robust Tracking of MPPT for Standalone/Grid Connected Power System. *Sustainability*, 2022, vol. 14, no. 15, art. no. 8986. doi: <https://doi.org/10.3390/su14158986>
- Sahraoui H., Mellah H., Drid S., Chrifi-Alaoui L. Adaptive maximum power point tracking using neural networks for a photovoltaic systems according grid. *Electrical Engineering & Electromechanics*, 2021, no. 5, pp. 57-66. doi: <https://doi.org/10.20998/2074-272X.2021.5.08>
- Khan S.A., Mahmood T., Awan K.S. A nature based novel maximum power point tracking algorithm for partial shading conditions. *Electrical Engineering & Electromechanics*, 2021, no. 6, pp. 54-63. doi: <https://doi.org/10.20998/2074-272X.2021.6.08>
- Saeed H., Mehmood T., Khan F.A., Shah M.S., Ullah M.F., Ali H. An improved search ability of particle swarm optimization algorithm for tracking maximum power point under shading conditions. *Electrical Engineering & Electromechanics*, 2022, no. 2, pp. 23-28. doi: <https://doi.org/10.20998/2074-272X.2022.2.04>
- Zaimi M., El Achoubi H., Ibral A., Assaid E.M. Determining combined effects of solar radiation and panel junction temperature on all model-parameters to forecast peak power and photovoltaic yield of solar panel under non-standard conditions. *Solar Energy*, 2019, vol. 191, pp. 341-359. doi: <https://doi.org/10.1016/j.solener.2019.09.007>
- Lahiouel Y., Latreche S., Khemliche M., Boulemzaoud L. Photovoltaic fault diagnosis algorithm using fuzzy logic controller based on calculating distortion ratio of values. *Electrical Engineering & Electromechanics*, 2023, no. 4, pp. 40-46. doi: <https://doi.org/10.20998/2074-272X.2023.4.06>
- Sathish C., Chidambaram I.A., Manikandan M. Intelligent cascaded adaptive neuro fuzzy interface system controller fed

- KY converter for hybrid energy based microgrid applications. *Electrical Engineering & Electromechanics*, 2023, no. 1, pp. 63-70. doi: <https://doi.org/10.20998/2074-272X.2023.1.09>.
13. Praveen Kumar T., Ganapathy S., Manikandan M. Improvement of voltage stability for grid connected solar photovoltaic systems using static synchronous compensator with recurrent neural network. *Electrical Engineering & Electromechanics*, 2022, no. 2, pp. 69-77. doi: <https://doi.org/10.20998/2074-272X.2022.2.10>.
14. Bengharbi A.A., Laribi S., Allaoui T., Mimouni A. Photovoltaic system faults diagnosis using discrete wavelet transform based artificial neural networks. *Electrical Engineering & Electromechanics*, 2022, no. 6, pp. 42-47. doi: <https://doi.org/10.20998/2074-272X.2022.6.07>.
15. Chen Y., Song L., Liu Y., Yang L., Li D. A Review of the Artificial Neural Network Models for Water Quality Prediction. *Applied Sciences*, 2020, vol. 10, no. 17, art. no. 5776. doi: <https://doi.org/10.3390/app10175776>.
16. Li X., Wen H., Hu Y., Jiang L. A novel beta parameter based fuzzy-logic controller for photovoltaic MPPT application. *Renewable Energy*, 2019, vol. 130, pp. 416-427. doi: <https://doi.org/10.1016/j.renene.2018.06.071>.
17. Loukil K., Abbes H., Abid H., Abid M., Toumi A. Design and implementation of reconfigurable MPPT fuzzy controller for photovoltaic systems. *Ain Shams Engineering Journal*, 2020, vol. 11, no. 2, pp. 319-328. doi: <https://doi.org/10.1016/j.asej.2019.10.002>.
18. Ilyas A., Khan M.R., Ayyub M. FPGA based real-time implementation of fuzzy logic controller for maximum power point tracking of solar photovoltaic system. *Optik*, 2020, vol. 213, art. no. 164668. doi: <https://doi.org/10.1016/j.ijleo.2020.164668>.
19. Rezk H., Aly M., Al-Dhaifallah M., Shoyama M. Design and Hardware Implementation of New Adaptive Fuzzy Logic-Based MPPT Control Method for Photovoltaic Applications. *IEEE Access*, 2019, vol. 7, pp. 106427-106438. doi: <https://doi.org/10.1109/ACCESS.2019.2932694>.
20. Vivek K., Subbarao K.V., Routray W., Kamini N.R., Dash K.K. Application of Fuzzy Logic in Sensory Evaluation of Food Products: a Comprehensive Study. *Food and Bioprocess Technology*, 2020, vol. 13, no. 1, pp. 1-29. doi: <https://doi.org/10.1007/s11947-019-02337-4>.
21. Chatrenour N., Razmi H., Doagou-Mojarrad H. Improved double integral sliding mode MPPT controller based parameter estimation for a stand-alone photovoltaic system. *Energy Conversion and Management*, 2017, vol. 139, pp. 97-109. doi: <https://doi.org/10.1016/j.enconman.2017.02.055>.
22. Akbar F., Mehmood T., Sadiq K., Ullah M.F. Optimization of accurate estimation of single diode solar photovoltaic parameters and extraction of maximum power point under different conditions. *Electrical Engineering & Electromechanics*, 2021, no. 6, pp. 46-53. doi: <https://doi.org/10.20998/2074-272X.2021.6.07>.
23. Benazza B., Bendaoud A., Slimani H., Benaissa M., Flitti M., Zeghoudi A. Experimental study of electromagnetic disturbances in common and differential modes in a circuit based on two DC/DC boost static converter in parallel. *Electrical Engineering & Electromechanics*, 2023, no. 4, pp. 35-39. doi: <https://doi.org/10.20998/2074-272X.2023.4.05>.
24. Lu C.-F., Liu C.-C., Wu C.-J. Dynamic modelling of battery energy storage system and application to power system stability. *IEE Proceedings - Generation, Transmission and Distribution*, 1995, vol. 142, no. 4, art. no. 429. doi: <https://doi.org/10.1049/ip-gtd:19951858>.
25. Moradi M.H., Reisi A.R. A hybrid maximum power point tracking method for photovoltaic systems. *Solar Energy*, 2011, vol. 85, no. 11, pp. 2965-2976. doi: <https://doi.org/10.1016/j.solener.2011.08.036>.
26. Sheetal W., Dubewar D. Comparative Study of Photovoltaic Array Maximum Power Point Tracking Techniques. *International Journal of Engineering Research and Technology*, 2015, vol. 4, no. 2, pp. 216-223.
27. Gounden N.A., Ann Peter S., Nallandula H., Krithiga S. Fuzzy logic controller with MPPT using line-commutated inverter for three-phase grid-connected photovoltaic systems. *Renewable Energy*, 2009, vol. 34, no. 3, pp. 909-915. doi: <https://doi.org/10.1016/j.renene.2008.05.039>.
28. Guenounou O., Dahhou B., Chabour F. Adaptive fuzzy controller based MPPT for photovoltaic systems. *Energy Conversion and Management*, 2014, vol. 78, pp. 843-850. doi: <https://doi.org/10.1016/j.enconman.2013.07.093>.
29. Mabrouk Y.A., Mokhtari B., Allaoui T. Frequency analysis of stator currents of an induction motor controlled by direct torque control associated with a fuzzy flux estimator. *Electrical Engineering & Electromechanics*, 2023, no. 6, pp. 27-32. doi: <https://doi.org/10.20998/2074-272X.2023.6.05>.
30. Altin N., Ozdemir S. Three-phase three-level grid interactive inverter with fuzzy logic based maximum power point tracking controller. *Energy Conversion and Management*, 2013, vol. 69, pp. 17-26. doi: <https://doi.org/10.1016/j.enconman.2013.01.012>.

Received 06.11.2023  
Accepted 26.03.2024  
Published 20.08.2024

Hadjer Bounechba<sup>1,2,3</sup>, Professor,  
Abdelfettah Boussaid<sup>1,2,4</sup>, Professor,  
Aissa Bouzid<sup>1,2</sup>, Professor,

<sup>1</sup> University Freres Mentouri Constantine 1,  
25000 Ain El Bey Way, Constantine, Algeria,

<sup>2</sup> Constantine Electrotechnical Laboratory,

<sup>3</sup> The Department of Electrical Engineering,

<sup>4</sup> Institut des Sciences et des Techniques Appliquees-ISTA,

e-mail: hadjer.bounechba@lec-umc.org (Corresponding Author);

abdelfettah.boussaid@lec-umc.org; aissa.bouzid@umc.edu.dz

#### How to cite this article:

Bounechba H., Boussaid A., Bouzid A. Experimental validation of fuzzy logic controller based on voltage perturbation algorithm in battery storage photovoltaic system. *Electrical Engineering & Electromechanics*, 2024, no. 5, pp. 20-27. doi: <https://doi.org/10.20998/2074-272X.2024.5.03>